Int J Adv Manuf Technol (2017) 92:3425–3433
DOI 10.1007/s00170-017-0359-1

ORIGINAL ARTICLE

Effect of rotation speed on microstructure and mechanical properties of refill friction stir spot welded 6061-T6 aluminum alloy

L. Zhou[1,2] · L. Y. Luo[1] · T. P. Zhang[1] · W. X. He[1] · Y. X. Huang[2] · J. C. Feng[1,2]

Received: 5 December 2016 / Accepted: 28 March 2017 / Published online: 26 April 2017

Abstract Refill friction stir spot welding (RFSSW) has been used to weld 6061-T6 aluminum alloy, and keyhole free joints were successfully obtained. Effect of tool rotation speed on microstructure and mechanical properties of joint was investigated. The joint was divided into four zones, i.e., the base material (BM), heat-affected zone (HAZ), thermo-mechanically affected zone (TMAZ), and stir zone (SZ) according to microstructural evolution. Defect was not found on the surface of welded joint, but inner defects of partial bonding, bonding ligament, hook, and voids were observed within the welded joint. The microhardness of HAZ and TMAZ was lower than that of the BM, while the maximum microhardness was obtained in the SZ of welded joints. With increasing tool rotation speed from 1100 to 1700 rpm, microhardness decreased with increasing grain size in the weld. The maximum tensile shear failure load of 7522 N was obtained for the joint under tool rotation speed of 1500 rpm. Two different failure modes of plug fracture and tensile-shear mixed fracture were observed during the tensile shear tests.

Keywords Refill friction stir spot welding · Keyhole · Microstructure · Mechanical properties

✉ L. Zhou
zhouli@hitwh.edu.cn

[1] Shandong Provincial Key Laboratory of Special Welding Technology, Harbin Institute of Technology at Weihai, Weihai 264209, People's Republic of China

[2] State Key Laboratory of Advanced Welding and Joining, Harbin Institute of Technology, Harbin 150001, People's Republic of China

1 Introduction

As a solid-state joining technology, friction stir spot welding (FSSW) can be divided into traditional FSSW (TFSSW) and refill FSSW (RFSSW). TFSSW proposed by Mazda Corporation of Japan [1] is a relatively new method. But the keyhole that inevitably remained at the center of the nugget limits the widespread applications of TFSSW. Meanwhile, the keyhole is an inherent defect itself, which will cause stress concentration and reduction of the effective connection area of the spot weld and impairs the mechanical properties of welded joint. RFSSW invented by Helmholtz-Zentrum Geesthacht (HZG) solved the problem [2], and the keyhole-free joint obtained by RFSSW has higher mechanical properties. Now, RFSSW is considered as a promising technology to replace riveting and resistance spot welding (RSW) [3–5].

The welding tool of RFSSW comprises of a clamping ring, a sleeve, and a pin, as shown in Fig. 1a. The clamping ring holds the plates against the anvil and prevents the material to overflow. The sleeve and pin have the same angular velocity, but with opposite movement along the axis direction during work. The process of RFSSW consists of four phases. In the first stage, the to-be-welded sheets are firmly pressed by the clamping ring and the anvil; the sleeve and the pin start to rotate at the same time (Fig. 1a). In the second stage, the sleeve plunges into the plates at a certain speed until it reaches a specified depth, and the pin moves up at the same time to create a space for accommodating the material extruded by the sleeve (Fig. 1b). In the third stage, the sleeve retracts back while the pin keeps moving down, so the plastic material can be refilled into the weld (Fig. 1c). In the fourth stage, once the pin and the

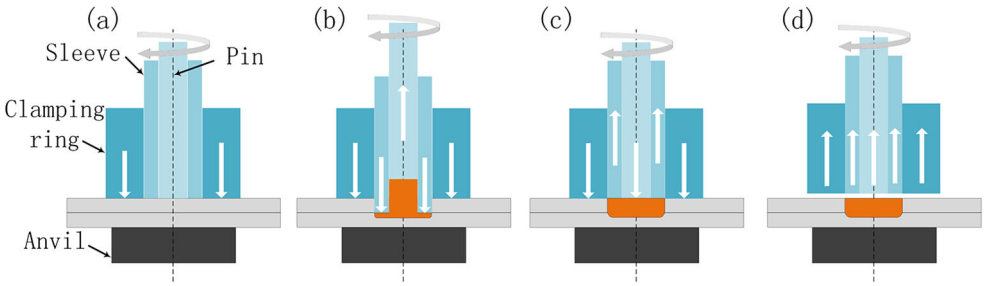

Fig. 1 Schematic illustration of RFSSW processes. **a** Stage 1. **b** Stage 2. **c** Stage 3. **d** Stage 4

sleeve reached at the same level, the process of RFSSW is ended (Fig. 1d) [2].

Until now, several studies have been done to understand the microstructure and mechanical properties of RFSSW joint, but detailed and comprehensive studies on microstructure and mechanical properties of RFSSW joint are relatively few. Li et al. [3] studied the fracture mechanism on RFSSW for 2021-T4 Al alloy and stated that sleeve plunge depth and heat input are important factors for determining tensile fracture modes. Amancio-Filho et al. [4] investigated the microstructure and mechanical behavior of 2024 Al alloy RFSSW joint. Tier et al. [5] found that shear strength for 5042 Al alloy RFSSW joint was influenced by stir zone morphology. Cao et al. [6] performed RFSSW on 6061-T6 Al alloy to study the hook formation and the mechanical properties. Shen et al. [7] performed the RFSSW experiment on 6061-T4 Al alloy to investigate the microstructure and mechanical properties of welded joint and reported that tool rotation speed played an important role in tensile shear load. Uematsu et al. [8] studied the influence of the refill probe hole and presented that the tensile strength of joint was improved by refilling process for Al-Mg-Si alloy. Rosendo et al. performed RFSSW on AA6181 Al alloy and investigated microstructure and mechanical properties of welded joint [9, 10]. Zhao et al. investigated process parameters on microstructure, mechanical properties, temperature, and material flow for RFSSWed alclad 7B04-T74 Al alloy [11–13]. Shen et al. [14] observed two fracture modes of shear fracture and plug fracture in 7075-T6 Al alloy RFSSW joint under different tool rotation speed.

In this paper, effect of tool rotation speed on microstructure and mechanical properties of RFSSWed 6061-T6 Al alloy was investigated in detail and the relation between microstructure, mechanical behavior, and process parameters was established.

2 Experimental procedure

The workpiece is 75 × 25 × 2-mm 6061-T6 Al alloy with chemical composition, and mechanical properties are listed in the Table 1, respectively. The RFSSW process was performed at the center of the overlap area of 25 × 25 mm between workpiece by a RFSSW machine developed in house, as shown in Fig. 2. The diameter of the champing ring, the sleeve, and the pin is 18, 9, and 5.3 mm, respectively. During the welding, the tool rotation speed ranging from 1100 to 1700 rpm was applied with constant sleeve plunge depth of 2.5 mm and plunge/retraction rate of 1 mm s^{-1}.

Transverse weld cross sections were cut by electrical discharge machining and prepared by standard metallographic procedure. The polished weld cross sections were etched with Keller's reagent. Metallographic analyses were carried out by Olympus GX51 optical microscopy (OM) to investigate the microstructural features and assess the quality of the joints produced under various RFSSW conditions. Tensile shear tests were carried out on INSTRON-1186 mechanical property testing machine with a crosshead displacement rate of 1 mm min^{-1}. To avoid the initial realignment, shims of the same thickness as the workpiece were used. Microhardness profiles were measured at the mid-thickness of the upper sheets and the bonding interfaces between sheets with a spacing of 0.5 mm between the indentations under test load of 0.98 N for 10 s. The tensile fracture morphologies were observed by a TESCAN VEGAII scanning electron microscopy (SEM).

3 Results and discussion

3.1 Characteristics of cross section in welded joint

The top view and the cross section of the typical weld produced at tool rotation speed of 1500 rpm are revealed in Fig. 3. It is clear that the keyhole is refilled completely and there is no defect on the surface except for slight indentation of tool, as shown in Fig. 3a. According to the characteristic of joint cross section, the weld is symmetrical with respect to the tool axis, as shown in Fig. 3b. Based on microstructural evolution, the weld can be divided into four regions, which are the base material (BM), heat-affected zone (HAZ),

Table 1 Chemical composition and mechanical properties of 6061-T6 Al alloys

Chemical compositions (wt.%)									Mechanical properties		
Mg	Si	Fe	Cu	Mn	Cr	Zn	Ti	Al	Tensile strength (MPa)	Elongation (%)	Hardness (HV)
0.8–1.2	0.4–0.8	0.7	0.15–0.4	0.15	0.04–0.35	0.25	0.5	Bal.	124	25	75–78

thermo-mechanically affected zone (TMAZ), and stir zone (SZ). Furthermore, three interface features, partial bonding, bonding ligament, and hook, are observed clearly in the joint cross section under tool rotation speed of 1500 rpm, as stated in Fig. 3b, which were caused by the inherent disadvantages of RFSSW [15].

The partial bonding (Fig. 4a) is a transition region bonding interface which belongs to inadequate bonding, while bonding ligament (Fig. 4b) is a region of good adhesion between interface of the upper and bottom sheets [16]. It must be pointed out that the partial bonding is an inclined zigzag line which indicates that the materials' flow and bonding ligament is redistributed as an arc-shape inside the weld. The hook is formed by the upward bending of the sheet interface due to the tool penetration into the bottom sheet (Fig. 4c, d). The upward bending of hook will reduce the effective thickness of the upper sheet, which impairs the mechanical properties of the joint [17, 18]. For the sake of the convenience, the upward bending height of the hook is expressed as H, which increases with tool rotation speed from 1100 to 1500 rpm and then decreases at the tool rotation speed of 1700 rpm according to Fig. 5. It could be argued that the dimensions of hook are controlled by heat input [6, 9], and relatively high tool rotation speed provides more heat to promote the vertical plastic flow of the material [12]. However, the excessive tool rotation speed may decrease the pressure gradient in the plasticized material and the values of H decrease.

Besides those interface features, the defect of void is observed in the joint at tool ration speed of 1100 rpm, as shown in Fig. 4e, while they disappear when the tool rotation increased to 1500 rpm (Fig. 4f). Zhao et al. [11] believed that the material loss in RFSSW plays an important role in formation of void. With increasing tool rotation speed, the heat input increases and the expanded volume of material is enough to make up the material loss. Oliveria et al. [19] attributed the formation of void to the thermal shrinkage, entrapped air, or some physical-chemical structural changes. Mishra suggested that the most critical stage in controlling fracture toughness is the control of the initiation of voids [20]. It is considered that particles provide interfaces that are easy initiation sites for voids, which induce stress concentration and provide crack initiation to deteriorate the mechanical properties of the welded joint.

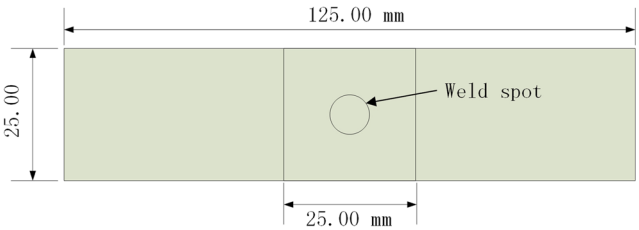

Fig. 2 Configuration and size of tensile shear specimen

3.2 Microstructure characterization in welded joint

Microstructural evolution in typical 6061-T6 Al alloy RFSSW joint is shown in Fig. 6. In the BM, the grains are elongated along the rolling direction (Fig. 6a). The HAZ only experiences the welding thermal cycle and no plastic deformation occurs in this zone during RFSSW, so microstructure in the HAZ is similar but slightly coarser compared to that in the BM (Fig. 6b). The TMAZ, located at the outside of sleeve moving path, is characterized by highly deformed grains in comparison to those in the BM and HAZ (Fig. 6c). Moderate deformation strain and moderate temperature are responsible for microstructural changes in TMAZ [9]. The SZ presents much finer equiaxed grains (Fig. 6d–f), which can be attributed to the dynamic recrystallization caused by high strain rate and high temperature during the process [21]. It should be noted that the grain size in SZ is not uniform, and the grain in SZ center (Fig. 6e) is coarser then those in SZ edge (Fig. 6d) and those in SZ top (Fig. 6f), which could be explained that the material in SZ edge and top suffers higher strain rate due to high linear velocity than in SZ center.

The effect of tool rotation speed on microstructure in 6061-T6 Al alloy RFSSW joint is shown in Fig. 7. There is little difference of grain morphology in HAZ, but the grain size is increased with increasing tool rotation speed due to increasing heat input, as shown in Fig.7a, b. And the deformation of the grains in the TMAZ is increased with the increase of tool rotation speed, as shown in

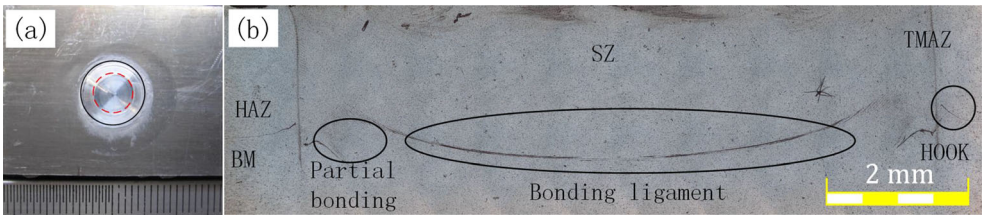

Fig. 3 Macroscopic appearance of RFSSW joint obtained at tool rotation speed of 1500 rpm. **a** Top view. **b** Cross section

Fig. 7c, d, which can be attributed to the increasing heat and shear stress. With the increasing tool rotation speed, the grain size in the SZ increases, as shown in Fig. 7e, f. The reason is that the higher welding heat input and longer cooling time facilitate the coarsening of the grains in the SZ during the cooling stage.

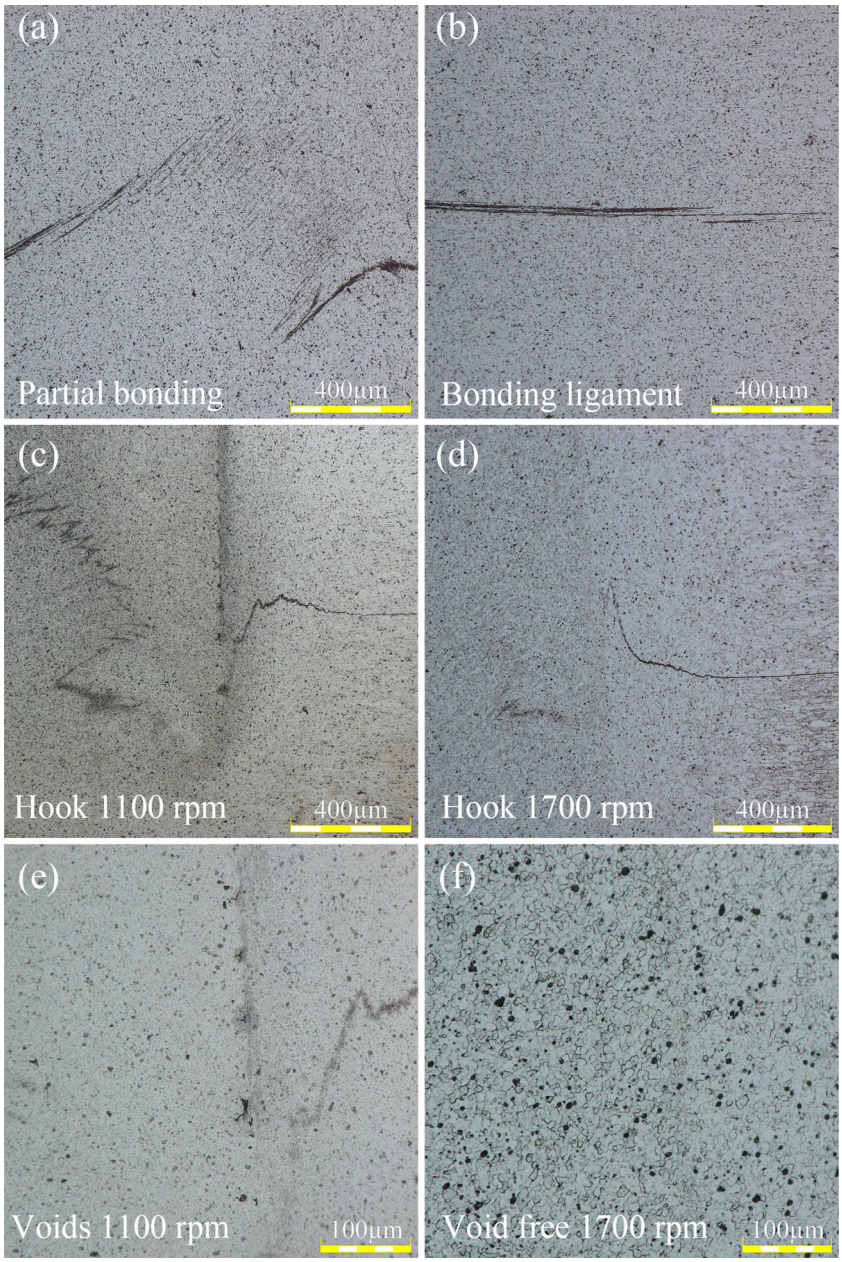

Fig. 4 Characteristics of the defects of the joint. **a** Partial bonding. **b** Bonding ligament. **c** Hook formed at 1100 rpm. **d** Hook formed at 1700 rpm. **e** Voids formed at 1100 rpm. **f** Void-free joint formed at 1700 rpm

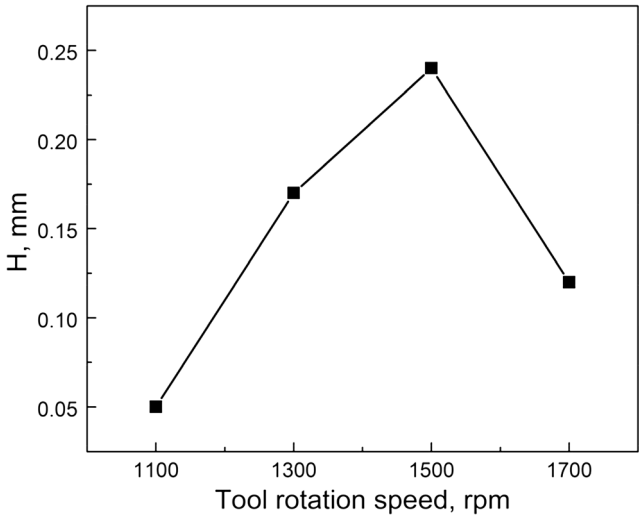

Fig. 5 Height of hook in weld joints obtained at different tool rotation speed

3.3 Microhardness distributions

The microhardness distribution at the mid-thickness of the upper sheet in 6061-T6 Al alloy RFSSW joints is revealed in Fig. 8a. The distribution of microhardness that is symmetric with respect to the centerline of the weld made at all given processing parameters with hardness of BM is about 75–78 HV. A softened region that comprises of TMAZ and HAZ exists in all the joints. It can be attributed to the thermal softening effect which is a typical characteristic for RFSSW of precipitate-hardened Al alloy [12, 21]. Compared with the TMAZ and HAZ, the SZ has much finer grains and precipitates. Therefore, the hardness in the SZ is higher than that in TMAZ and HAZ. It should be noted that the hardness in the edge of SZ is the maximum within the joint, as shown by arrow in Fig. 8a. The reason for this is that this region subjected to more severe plastic deformation because of higher velocity at the periphery of sleeve, so grains in this region are even smaller. With the increasing tool rotation speed, the hardness of SZ decreases. The corresponding duration of cooling stage is longer at the higher tool rotation speed, which increases the size of recrystallized grain and precipitated phase, and thus, the effect of grain refinement strengthening and precipitation strengthening decreases. It could be deduced that relatively higher hardness can be obtained in the SZ under the relatively low tool rotation speed.

The microhardness distribution at the bonding interface of the RFSSW joint under different tool rotation speed is shown in Fig. 8b, which is unstable and fluctuates wildly. The hardness in TMAZ of bonding interface is very low due to the existence of hook and partial bonding. It should be noted that the hardness in SZ edge at the interface significantly decreases compared with that in mid-thickness of the upper sheet, which attributed the decrease to lower peak temperature and shorter thermal cycle duration [7].

3.4 Tensile shear properties and fracture mode

The tensile shear failure loads of the joints welded at different tool rotation speed is shown in Fig. 9. The tensile shear failure load increases to the maximum 7522 N with increasing tool rotation speed from 1100

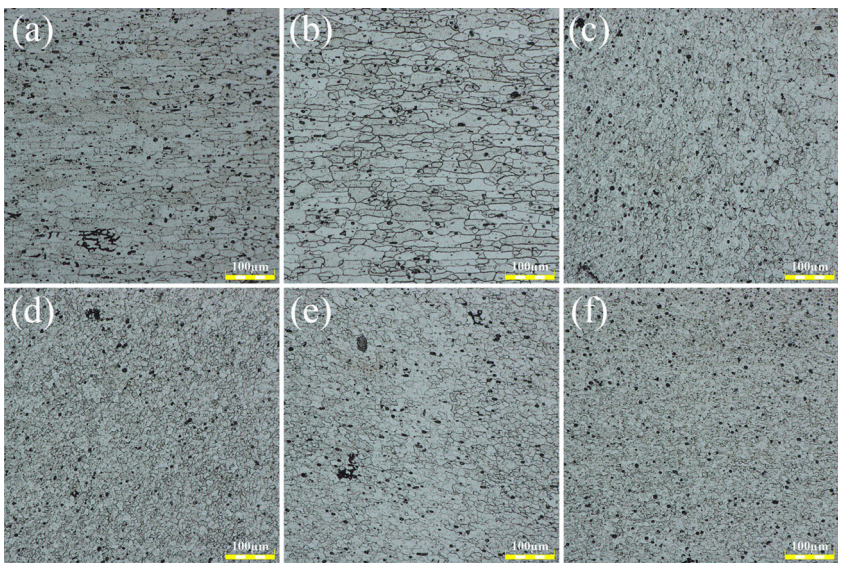

Fig. 6 Typical microstructure in 6061-T6 Al alloy RFSSW joint. **a** BM. **b** HAZ. **c** TMAZ. **d** SZ edge. **e** SZ center. **f** SZ top

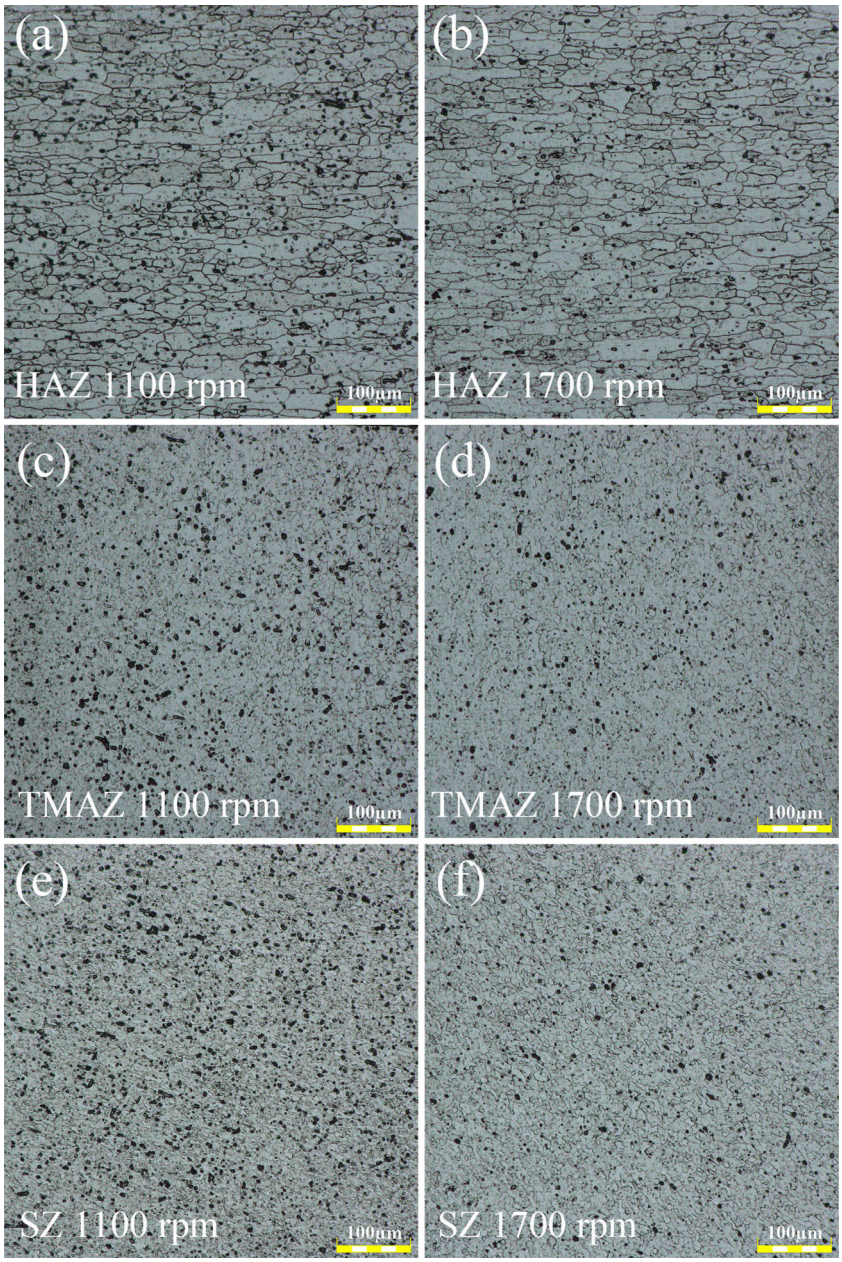

Fig. 7 Grain structures in different microstructural zone at different tool rotation speed. **a** HAZ formed at 1100 rpm rpm. **b** HAZ formed at 1700 rpm. **c** TMAZ formed at 1100 rpm. **d** TMAZ formed at 1700 rpm. **e** SZ formed at 1100 rpm. **f** SZ formed at 1700 rpm

to 1500 rpm, and then, it decreases at 1700 rpm. The tensile shear failure load of the joint is controlled by heat input which is mostly affected by rotation speed and joining time [10, 22]. It should be noted that voids formed in SZ/TMAZ interface at the tool rotation speed of 1100 rpm for insufficient heat input induce stress concentration and provide crack initiation, and thus, the tensile shear failure load is low. However, the tensile shear failure load decreases due to the lower hardness of the SZ at the tool rotation speed of 1700 rpm [11].

Two typical fracture modes of plug fracture and tensile shear fracture for tensile shear test specimen of welded joint under different tool ration speed are presented in Fig. 10. The plug fracture (Fig. 10a) can be observed when the tool rotation speed is lower than 1500 rpm, while the tensile shear fracture (Fig. 10b) is shown under higher tool rotation speed. In addition, the tensile shear loads of tensile shear fracture joint are relatively higher than those of plug fracture joint, as indicated by Fig. 9.

In plug fracture, the crack initiates at hook tip which bears the largest load because of stress concentration and propagates upward along nugget periphery into the upper sheet and circularly along the nugget to other side at the same time. Then, the crack propagates downward

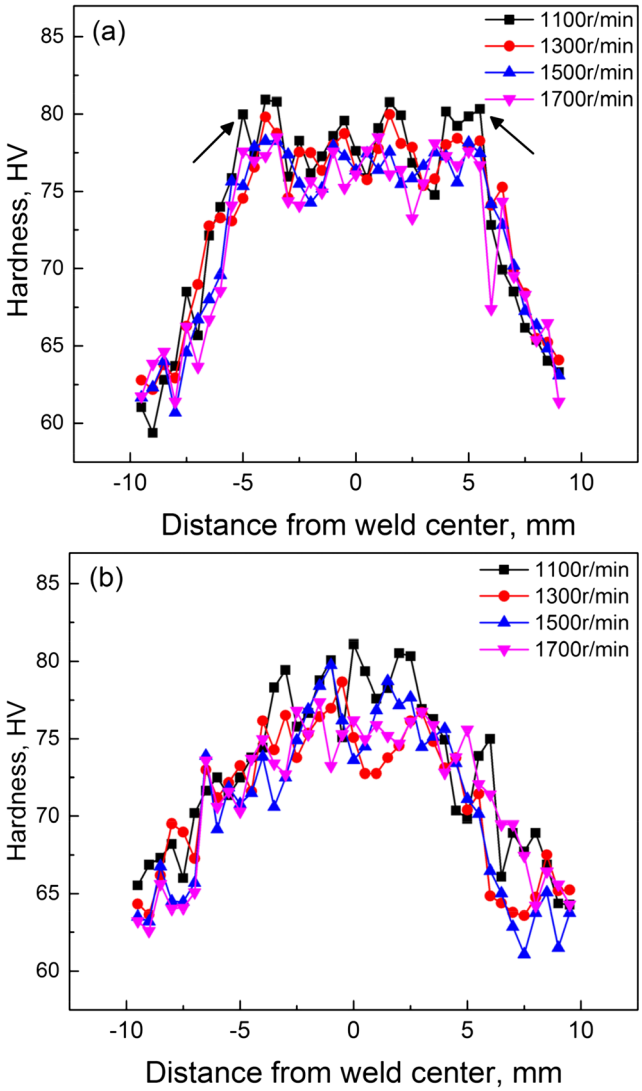

Fig. 8 Microhardness distributions at (**a**) the mid-thickness of the upper sheet and (**b**) the bonding interface between sheets

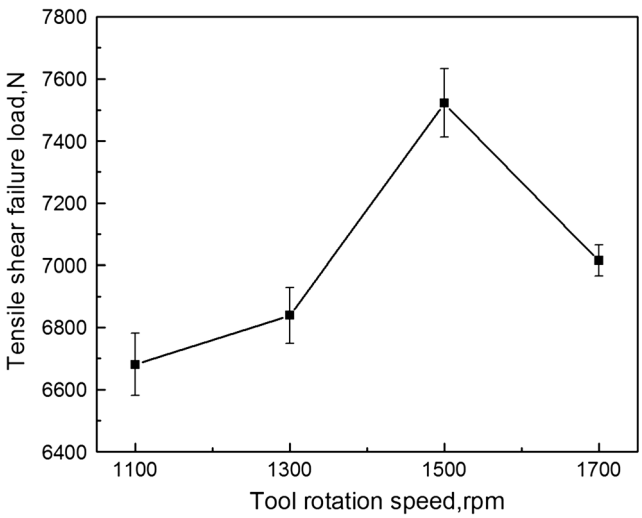

Fig. 9 Tensile shear failure loads of the RFSSW welded joints at different tool rotation speed

along the SZ/TMAZ interface to bottom sheet for which the hook geometry and the void in the SZ/TMAZ interface are responsible, as shown in Fig. 4e. Finally, the crack propagates into upper sheet causing fracture [2, 5]. To investigate the fracture micromorphology, SEM micrographs taken from the fractured surface are shown in Fig. 11. Figure 11a reveals the overall fracture surface of the plug fracture (marked by red frame in Fig. 10a), and the magnification regions highlighted from B–E in Fig. 11a are indicated in Fig. 11b–e. Region B locates on the bottom sheet, while D take from the interface and C and E locate on the upper sheet. Region B is characterized by elongated dimples (Fig. 11b), which are caused by shear stress distributed along the vertical direction [14]. Region C exhibits striation pattern, which can be attributed to the crack annular propagation [7]. Numerous equiaxed dimples were observed in region D exhibit (Fig. 11d), which can be explained by the deformation of the specimen, and then, the deformation causes the direction of crack propagation perpendicular to tensile shear load which is equivalent to positive stress [3]. Region E is composed of smooth surface and striation marks due to the interaction between the sleeve and material [20].

Tensile shear fracture shares some similarity in crack initiation and propagation with plug fracture except the propagation of crack in the final fracture position [7]. The crack only propagates along the hook into the nugget in the final facture position, so the fracture presents a slope in nugget [2]. SEM micrographs of overall fracture in slope of nugget (marked by red frame in Fig. 10b) are revealed in Fig. 12a. The high-magnification regions from B–E marked in Fig. 12a, c are exhibited in Fig. 12b–e. As shown in Fig. 12b, region B is the initiation of crack located at hook. The crack in region B indicates that crack has two potential propagation paths in final fracture position, which are upward hook and the SZ/TMAZ interface in bottom sheet. In tensile shear fracture mode, the bonding strength of the SZ/TMAZ interface is high due to void-free and so the upward hook becomes the crack propagation path [23, 24]. As shown in Fig. 12c, d, regions C and D show the similar fracture mechanism, which occurred due to brittle fracture. Dimples are not observed on fracture surface which indicates that plastic deformation does not occur before fracture. To confirm the fracture mode in slope, we take the higher-magnification SEM micrograph (Fig. 12e), which show lots of microdimples and polyhedron morphology indicating that fracture is intergranular fracture. The possible reason for intergranular fracture is that the precipitate assembled on grain boundary in reprecipitated stage.

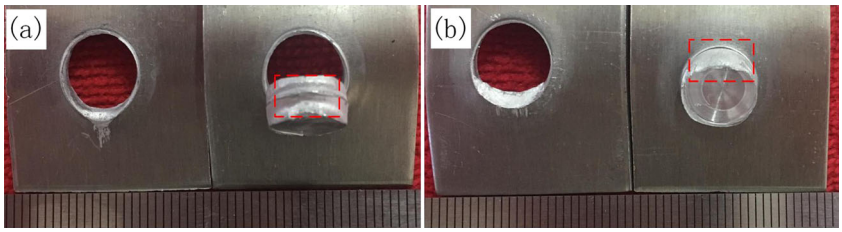

Fig. 10 The typical tensile shear fracture mode of joints obtained at different tool rotation speed

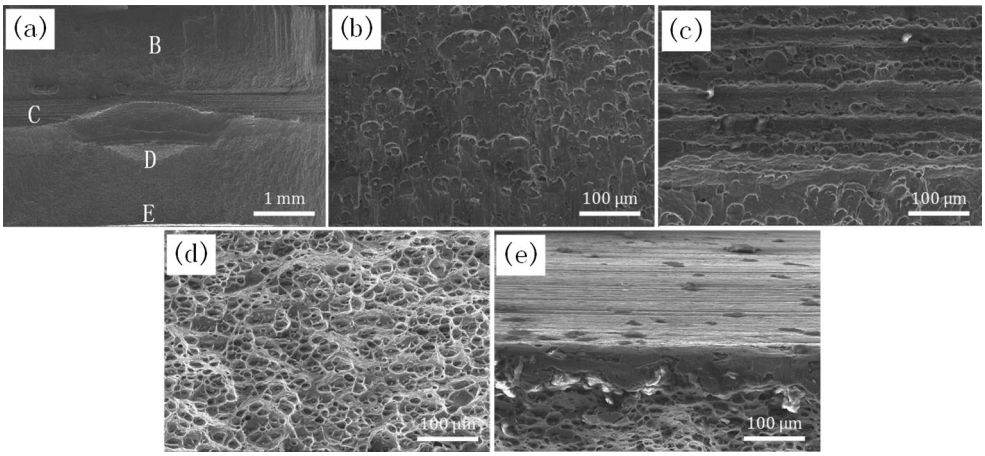

Fig. 11 SEM of **a** the plug fracture surface and **b**–**e** the locations *B*–*E* in Fig. 10a, respectively

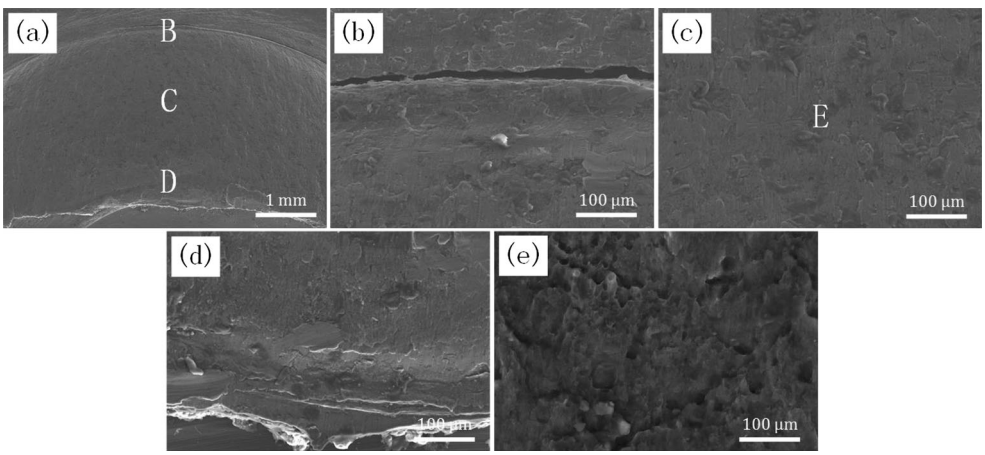

Fig. 12 SEM of **a** the plug shear fracture surface on nugget and **b**–**d** magnified view from regions *B*–*D* marked in Fig. 11a, e magnified view from region *E* marked in Fig. 11c

4 Conclusion

In the present study, effect of rotation speed on microstructure and mechanical properties of 6061 aluminum alloy RFSSW joints is investigated. The weld cross section is divided into four sections of BM, TMAZ, HAZ, and SZ. The grain in the SZ is the finest and the TMAZ is characterized by highly deformed grains. The grains in the HAZ are coarser compared with those in the BM due to the effect of thermal cycle. The coarser grains are generally formed in all zones of weld with increasing tool rotation speed. The defects such as partial bonding, bonding ligament, and hook are observed at the interface of all joints, and the voids are located at SZ/TMAZ interface in the weld obtained at lower rotation speed. A soften region that consists of HAZ and TMAZ is developed in the joint with the minimum hardness in the HAZ and the maximum hardness located in the SZ. With the increasing tool rotation speed from 1100 to 1500 rpm, the tensile shear failure load increases to the maximum value of 7522 N and then it decreases significantly at tool rotation speed of 1700 rpm. The plug fracture mode is found when the tool rotation speed is lower than 1500 rpm, while tensile shear fracture mode is developed when the tool rotation speed is 1500 rpm or even higher. The plug fracture is characterized by dimple and the tensile shear fracture is polyhedron morphology by SEM.

Acknowledgements The research was sponsored by the State Key Lab of Advanced Welding and Joining, Harbin Institute of Technology (Grant No. AWJ-M13-11), the Indigenous Innovation and Achievement Transformation Program of Shandong Province (Grant No. 2014CGZH1003), the Key Research & Development program of Shandong Province (2015GGX103002), Production-Study-Research Cooperative Innovation Demonstration Project Foundation of Weihai City (Grant No. 2014CXY02), and the Science and Technology Development Program of Weihai City (Grant No. 2014DXGJ17).

References

1. Iwashita T (2003) Method and apparatus for joining. US Patent 6601751:B2
2. Schilling C, Dos Santos JF (2001) Method and device for linking at least two adjoining work pieces by friction welding. US Patent 6722556:B2
3. Li Z, Ji S, Ma Y, Yue Y, Gao S (2016) Fracture mechanism of refill friction stir spot-welded 2024-T4 aluminum alloy. Int J Adv Manuf Technol 86(5–8):1925–1932
4. Amancio-Filho ST, Camillo APC, Bergmann L, dos Santos JF, Kury SE, Machado NGA (2011) Preliminary investigation of the microstructure and mechanical behaviour of 2024 aluminium alloy friction spot welds. Mater Trans 52(5):985–991
5. Tier MD, Rosendo TS, dos Santos JF, Huber H, Mazzaferro JA, Mazzaferro CP, Strohaecker TR (2013) The influence of refill FSSW parameters on the microstructure and shear strength of 5042 aluminium welds. J Mater Process Technol 213(6):997–1005
6. Cao JY, Wang M, Kong L, Guo LJ (2016) Hook formation and mechanical properties of friction spot welding in alloy 6061-T6. J Mater Process Technol 230:254–262
7. Shen Z, Yang X, Yang S, Zhang Z, Yin Y (2014) Microstructure and mechanical properties of friction spot welded 6061-T4 aluminum alloy. Mater Des 54:766–778
8. Uematsu Y, Tokaji K, Tozaki Y, Kurita T, Murata S (2008) Effect of re-filling probe hole on tensile failure and fatigue behaviour of friction stir spot welded joints in Al–Mg–Si alloy. Int J Fatigue 30(10–11):1956–1966
9. Rosendo T, Parra B, Tier MAD, da Silva A, dos Santos JF, Strohaecker TR (2011) Mechanical and microstructural investigation of friction spot welded AA6181-T4 aluminium alloy. Mater Des 32(3):1094–1100
10. Rosendo T, Tier M, Mazzaferro J, Mazzaferro C, Strohaecker TR, dos Santos JF (2015) Mechanical performance of AA6181 refill friction spot welds under lap shear tensile loading: mechanical performance of aa6181 refill friction spot welds under lap shear tensile loading. Fatigue Fract Eng Mater Struct 38(12):1443–1455
11. Zhao YQ, Liu HJ, Chen SX, Liu Z, Hou JC (2014) Effects of sleeve plunge depth on microstructures and mechanical properties of friction spot welded Alclad 7B04-T74 aluminum alloy. Mater Des 62: 40–46
12. Zhao YQ, Liu HJ, Lin Z, Chen SX, Hou CJ (2014) Microstructures and mechanical properties of friction spot welded Alclad 7B04-T74 aluminium alloy. Sci Technol Weld Join 19(7):617–622
13. Zhao Y, Liu H, Yang T, Liu Z, Hu Y (2016) Study of temperature and material flow during friction spot welding of 7B04-T74 aluminum alloy. Int J Adv Manuf Technol 83(9–12):1467–1475
14. Shen Z, Yang X, Zhang Z, Cui L, Li T (2013) Microstructure and failure mechanisms of refill friction stir spot welded 7075-T6 aluminum alloy joints. Mater Des 44:476–486
15. Shen Z, Yang X, Zhang Z, Cui L, Yin Y (2013) Mechanical properties and failure mechanisms of friction stir spot welds of AA 6061-T4 sheets. Mater Des 49:181–191
16. Tier MD, Rosendo TS, Mazzaferro JA, Mazzaferro CP, dos Santos JF, Strohaecker TR (2016) The weld interface for friction spot welded 5052 aluminium alloy. Int J Adv Manuf Technol 1–10
17. Yin YH, Ikuta A, North TH (2010) Microstructural features and mechanical properties of AM60 and AZ31 friction stir spot welds. Mater Des 31(10):4764–4776
18. Badarinarayan H, Shi Y, Li X, Okamoto K (2009) Effect of tool geometry on hook formation and static strength of friction stir spot welded aluminum 5754-O sheets. Int J Mach Tools Manuf 49(11): 814–823
19. Oliveira PHF, Amancio-Filho ST, dos Santos JF, Hage E Jr (2010) Preliminary study on the feasibility of friction spot welding in PMMA. Mater Lett 64(19):2098–2101
20. Mishra RS, Ma ZY (2005) Friction stir welding and processing. Mater Sci Eng R Rep 50:1–78
21. Rodrigues DM, Loureiro A, Leitao C, Leal RM, Chaparro BM, Vilaca P (2009) Influence of friction stir welding parameters on the microstructural and mechanical properties of AA 6016-T4 thin welds. Mater Des 30(6):1913–1921
22. Su P, Gerlich A, North TH, Bendzsak GJ (2013) Energy utilisation and generation during friction stir spot welding. Sci Technol Weld Join 11(2):163–169
23. Effertz PS, Infante V, Quintino L, Sunhuddin U, Hanke S, dos Santos JF (2016) Fatigue life assessment of friction spot welded 7050-T76 aluminium alloy using Weibull distribution. Int J Fatigue 87:381–390
24. Ji SD, Wang Y, Zhang J, Li Z (2016) Influence of rotating speed on microstructure and peel strength of friction spot welded 2024-T4 aluminum alloy. Int J Adv Manuf Technol 1–7